Available online at www.sciencedirect.com
SCIENCE DIRECT®
Journal of Solid State Chemistry 178 (2005) 1087–1093
JOURNAL OF SOLID STATE CHEMISTRY
www.elsevier.com/locate/jssc

The new semiconducting polychalcogenide Ba_2SnSe_5 exhibiting Se_3^{2-} units and distorted $SnSe_6$ octahedra

Abdeljalil Assoud, Navid Soheilnia, Holger Kleinke*

Department of Chemistry, University of Waterloo, Waterloo, Ont., Canada N2L 3G1

Received 18 November 2004; received in revised form 11 January 2005; accepted 13 January 2005

Abstract

The new polyselenide Ba_2SnSe_5 was prepared from the elements under exclusion of air at temperatures between 650 and 750 °C. Ba_2SnSe_5 crystallizes in the orthorhombic space group $P2_12_12_1$, with the lattice parameters of $a = 12.3572(8)$ Å, $b = 17.235(1)$ Å, $c = 18.134(1)$ Å, $V = 3862.1(4)$ Å^3 ($Z = 16$). Its structure comprises nonlinear Se_3^{2-} trimers, isolated $SnSe_4$ tetrahedra and trimeric Sn_3Se_{10} units, the latter consisting of a central (distorted) $SnSe_6$ octahedron sharing two opposite basal edges with two $SnSe_4$ tetrahedra. The structural differences to its Sr and Te analogs, Sr_2SnSe_5 and both modifications of Ba_2SnTe_5, are intriguing, and illustrated in detail in this article. Ba_2SnSe_5 is a dark brown semiconductor with a computed band gap of 1.2 eV.

Keywords: Polychalcogenide; Stannate; Selenide; Crystal structure; Electronic structure; Semiconductor

1. Introduction

Quite recently we commenced to investigate tin polychalcogenides with the intent of evaluating their use for the thermoelectric energy conversion. This area in general has enjoyed impressive success in the past years [1–5]. Common knowledge dictates that good thermoelectrics are semiconductors forming complex crystal structures with heavy constituent elements [6,7], and calculations revealed that their band gaps ideally encompass $6–10\,k_BT$, with k_B = Boltzmann constant, T = operating temperature [8]. This range corresponds to band gaps between 0.16 and 0.26 eV at room temperature.

On our quest for narrow gap semiconductors we published two Sn polychalcogenides in the year 2004, Sr_2SnSe_5 [9] and a new modification of Ba_2SnTe_5 [10] with calculated band gaps of 0.9 eV and 0.25 eV, respectively. In the latter case, we experimentally deduced the band gap to be 0.18 eV from temperature dependent electrical conductivity measurements. Both of these compounds form crystal structures with quite unique motifs, namely unusually distorted Sn–Se polyhedra in Sr_2SnSe_5, and distorted $SnTe_5$ trigonal bipyramids and a nonclassical Te_5^{4-} unit in Ba_2SnTe_5. Electronic structure calculations were performed on the former by Hoffmann et al. because of the peculiar geometry around one Sn site, based on unpublished concurrent data from Johrendt et al. [11]. Later in 2004, the related $Sr_4Sn_2Se_9$ was introduced in detail [12]. So far, the Ba–Sn–Se system remained literally unexplored. With this contribution, we present the new polyselenide Ba_2SnSe_5, formally isovalent with Sr_2SnSe_5 and Ba_2SnTe_5 but exhibiting different structure motifs.

2. Experimental

2.1. Synthesis and analysis

The elements were acquired either in pieces (Ba: 99% nominal purity, ALDRICH) or in powder form (Sn: 99.8%, −325 mesh, ALFA AESAR; Se: 99.5%, −100

*Corresponding author. Fax: +1 519 746 0435.
E-mail address: kleinke@uwaterloo.ca (H. Kleinke).

0022-4596/$ - see front matter © 2005 Elsevier Inc. All rights reserved.
doi:10.1016/j.jssc.2005.01.011

mesh, ALDRICH). Ba_2SnSe_5 was prepared starting from the elements in the stoichiometric ratio of 2:1:5. This mixture was placed into a fused silica tube, which was then sealed under vacuum. The tube was put into a resistance furnace, heated to 750 °C within three days, kept at 750 °C for four days, cooled down to 700 °C within ten minutes, and then annealed at 650 °C for four days. In the final step, the furnace was cooled down to room temperature within four days. The brown–black reaction mixture appeared to be homogenous. The powder diagram obtained utilizing the INEL powder diffractometer with position-sensitive detector (Cu$K\alpha_1$ radiation) gave no hint to the formation of any known binary compound. After the successful structure determination described below we verified that Ba_2SnSe_5 was obtained in quantitative yields.

We performed an EDX investigation (EDX: energy dispersive analysis of X-rays) using an electron microscope (LEO 1530) with an additional EDX device (EDAX Pegasus 1200). The scans were performed with an acceleration voltage of 21 kV under high dynamic vacuum. No impurities (e.g., stemming from the reaction container) were detected. Taking the Lα peaks of Ba, Sn, and Se (at 4.465 keV, 3.443 keV and 1.419 keV, respectively) into account for the (standardless) quantitative analysis, the Ba:Sn:Se ratios were calculated to be 23:11:66 at% (averaged over three crystals). This compares reasonably well with the ratio of 25:12.5:62.5 expected based on the 2–1–5 stoichiometry.

2.2. Crystal structure study

A bar-shaped dark brown crystal was mounted onto the Smart APEX CCD (BRUKER, utilizing Mo$K\alpha$ radiation). The scans of 0.3° in ω were done in two groups of 606 frames (each with an exposure time of 60 s) at $\phi = 0°$ and 60°. The data were corrected for Lorentz and polarization effects. Absorption corrections were based on fitting a function to the empirical transmission surface as sampled by multiple equivalent measurements using SADABS [13].

The structure solution and refinement were carried out with the SHELXL package [14]. We expected orthorhombic symmetry based on the three 90° angles, and $a \neq b \neq c$. This was verified by the internal R value of 4.2% in the orthorhombic crystal system. The systematic absences were unambiguous, limiting the possible space groups to one, namely $P2_12_12_1$. The structure solution (Direct Methods) in this space group was successful, yielding 32 independent atom sites. The 20 sites occupied by clearly the lightest atom were assigned to be Se positions. Then the sites with no contacts to Se atoms <3 Å were identified as Ba positions, and the remaining four sites all exhibited bonds to Se atoms starting at 2.5 Å, typical for Sn^{IV} atoms. This model was confirmed by the uniform distribution of equivalent displacement factors, all being of the order of 0.01 Å^2. The final refinement converged with an acceptable residual factor of $R_w(F_o^2) = 7.8\%$ (all data). Details of the structure determination are given in Table 1, and atomic positions with equivalent displacement parameters may be found in Table 2. Further details of the crystal structure investigation can be obtained from the Fachinformationszentrum Karlsruhe, 76344 Eggenstein-Leopoldshafen, Germany, on quoting the depository number CSD-414418.

Table 1
Crystal data and structure refinement of Ba_2SnSe_5

Empirical formula	Ba_2SnSe_5
Formula weight (g/mol)	788.17
Temperature (K)	298(2)
Wavelength (Å)	0.71073
Space group	$P2_12_12_1$
Cell dimensions	
a (Å)	12.3572(8)
b (Å)	17.235(1)
c (Å)	18.134(1)
V (Å^3)	3862.1(4)
No. of formula units per cell	16
Calculated density (g/cm^3)	5.422
Absorp. coeff. (mm^{-1})	29.40
$F(000)$	5312
Crystal size (μm)	$80 \times 78 \times 25$
2θ range	3.26–60.0
Reflections collected	32119
Independent reflections (R_{int})	11107 (0.042)
Observed reflections\refined parameters	9435\291
Absorption correction	Empirical
Min./max transmission	0.77/1
Goodness-of-fit on F^2	1.25
$R(F)$, $R_w(F^2)$ ($I > 2\sigma(I)$)	0.055, 0.075
$R(F)$, $R_w(F^2)$ (all data)	0.067, 0.078
Extinction coefficient	0.000034(3)
Max. diff. peak, hole (e/Å^3)	2.76, −2.50

2.3. Electronic structure calculation

The band structure of Ba_2SnSe_5 was calculated employing the self-consistent tight-binding *first principles* LMTO approximations (LMTO = linear muffin tin orbitals [15,16]). In the LMTO approach, the density functional theory is used with the local density approximation (LDA) [17]. The integration in k space was performed by an improved tetrahedron method [18] on a grid of 92 irreducible k points of the first Brillouin zone. Integrated COHP values of selected bonds were extracted from the energy-partitioning Crystal Orbital Hamilton Population scheme [19] to gain information about the bond strengths, comparable to the longer established Mulliken Overlap Populations [20] extracted from the Crystal Orbital Overlap Populations [21].

Table 2
Atomic coordinates and equivalent displacement parameters of Ba_2SnSe_5

Atom	x	y	z	$U_{eq}/Å^2$
Ba1	0.36392(7)	0.17696(4)	0.00290(4)	0.01098(16)
Ba2	0.35890(7)	0.17831(4)	0.25424(4)	0.01131(16)
Ba3	0.49582(7)	0.42713(4)	0.74393(4)	0.01061(16)
Ba4	0.48992(7)	0.43262(4)	0.49505(4)	0.01091(16)
Ba5	0.36648(7)	0.17654(4)	0.75223(4)	0.01079(16)
Ba6	0.86690(7)	0.31800(4)	0.49689(4)	0.01149(16)
Ba7	0.00565(7)	0.56863(5)	0.74664(4)	0.01202(17)
Ba8	0.00594(7)	0.57018(5)	0.49446(4)	0.01160(17)
Sn1	0.18608(7)	0.37434(5)	0.87227(5)	0.01538(17)
Sn2	0.18095(7)	0.36774(5)	0.07380(5)	0.01277(18)
Sn3	0.67839(7)	0.13009(5)	0.32934(5)	0.01124(18)
Sn4	0.15057(6)	0.31601(4)	0.36210(5)	0.00921(16)
Se1	0.35638(9)	0.32662(6)	0.37090(7)	0.0123(2)
Se2	0.36091(9)	0.32428(6)	0.12441(7)	0.0123(2)
Se3	0.01458(10)	0.42533(6)	0.36916(8)	0.0123(2)
Se4	0.50851(10)	0.07427(7)	0.87817(8)	0.0121(3)
Se5	0.37747(9)	0.31577(6)	0.87290(7)	0.0100(2)
Se6	0.85666(10)	0.17379(7)	0.38085(7)	0.0126(3)
Se7	0.49115(9)	0.07479(6)	0.13126(8)	0.0105(2)
Se8	0.61984(11)	0.23906(7)	0.24368(7)	0.0132(3)
Se9	0.18919(10)	0.10163(6)	0.12828(8)	0.0129(2)
Se10	0.50828(10)	0.07515(7)	0.38330(7)	0.0132(3)
Se11	0.23959(11)	0.47585(7)	0.76077(7)	0.0121(3)
Se12	0.62084(11)	0.23698(7)	0.01859(7)	0.0111(3)
Se13	0.19057(10)	0.10201(7)	0.38456(7)	0.0128(3)
Se14	0.18849(10)	0.10708(6)	0.87936(7)	0.0125(3)
Se15	0.24001(11)	0.47496(7)	0.98323(7)	0.0129(3)
Se16	0.81077(10)	0.60820(6)	0.87257(8)	0.0137(3)
Se17	0.24909(11)	0.99666(7)	0.05314(7)	0.0114(3)
Se18	0.25075(11)	0.99722(7)	0.30416(7)	0.0116(3)
Se19	0.11120(11)	0.23874(7)	0.47773(7)	0.0127(3)
Se20	0.11061(11)	0.25039(7)	0.24014(7)	0.0115(3)

2.4. Resistance measurement

We pressed part of the ground phase-pure sample into a bar-shaped pellet of the dimensions $6 \times 1 \times 1$ [in mm] for physical transport measurements, since no single crystals of sufficient dimensions were available. The high internal resistance of the pellet inhibited Seebeck and electrical resistance measurements. Based on our experiences with other high resistance materials, we conclude that the specific resistance of the as-cast Ba_2SnSe_5 sample must be above 100 kΩ cm at room temperature.

3. Results and discussion

3.1. Crystal structure

The polyselenide Ba_2SnSe_5 crystallizes in a new structure type. This structure contains a trimeric Sn_3Se_{10} unit, an additional, not connected $SnSe_4$ tetrahedron, and bent Se_3^{2-} units. Fig. 1 reveals how these motifs are embedded in the matrix of the cations, here Ba^{2+}, compared to the corresponding, but in part different structure motifs of Sr_2SnSe_5 [9].

Each Sr^{2+} and each Ba^{2+} cation are surrounded by nine Se atoms, with Sr–Se distances ranging from 3.12 to 3.37 Å, and Ba–Se distances being between 3.24 and 3.70 Å, the vast majority of the latter between 3.3 and 3.5 Å. The stacking of Sr^{2+} and Ba^{2+}, forming linear chains parallel to the c-axis, is topologically equivalent in Sr_2SnSe_5 and Ba_2SnSe_5. Correspondingly, the cell dimensions are quite comparable, with Ba_2SnSe_5 exhibiting slightly larger cell parameters because of the larger cation, and a doubled c-axis: the values in Å are $a = 12.4$, $b = 17.2$, $c = 18.1$ for Ba_2SnSe_5, and $a = 12.1$, $b = 16.6$, $c = 8.6$ for Sr_2SnSe_5. In both cases, the Se_3^{2-}

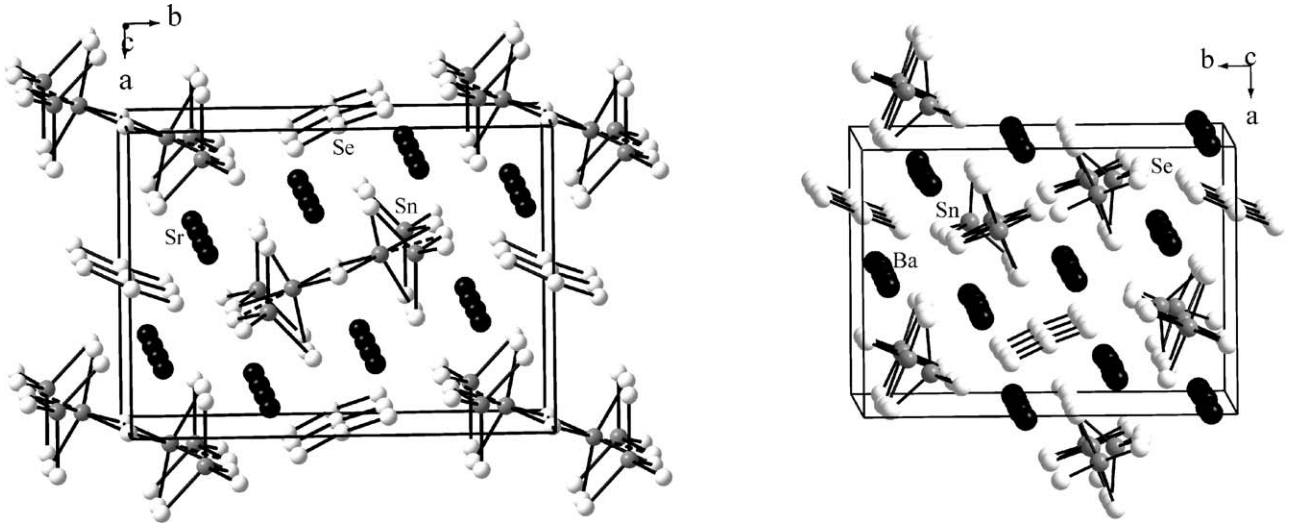

Fig. 1. Crystal structures of Sr_2SnSe_5 (left) and Ba_2SnSe_5 (right).

units are stacked on top of each other to fill an almost square channel formed by the cations. Its dimensions (from cation to cation) are 4.46 Å × 4.83 Å in Sr_2SnSe_5, and 4.62 Å × 4.94 Å in Ba_2SnSe_5.

Similarly, a rectangular channel of the cation chains, which runs along the *c*-axis as well, surrounds the Sn–Se polyhedra. Its dimensions are 4.45 Å × 6.45 Å in Sr_2SnSe_5, and 4.63 Å × 6.65 Å in Ba_2SnSe_5. An evident difference between these two structures is that the Sn–Se polyhedra in Sr_2SnSe_5 share an edge with its counterparts of the neighboring Sr channel, while the ones in Ba_2SnSe_5 are not interconnected in that direction. In Ba_2SnSe_5, $SnSe_4$ tetrahedra alternate with the trimeric Sn_3Se_{10} units along the *c*-axis (Fig. 2). Two of these columnar motifs run side by side—without sharing common atoms—within neighboring channels of Ba^{2+} cations, while the C-shaped tetrameric Sn_4Se_{14} unit of Sr_2SnSe_5 extends itself into two channels of Sr^{2+} cations. The more pronounced condensation in the *a*,*b* plane of Sr_2SnSe_5, ultimately connected to the different Sn–Se polyhedra, may be a consequence of the smaller cation matrix surrounding the Sn–Se units. As well, the C-shaped unit of Sr_2SnSe_5 repeats itself after 8.64 Å, while the alternating Sn_3Se_{10} and $SnSe_4$ units of Ba_2SnSe_5 are repeated every 18.1 Å, i.e., averaged 4.53 Å per Sn atom, compared to 4.32 Å in Sr_2SnSe_5. Moreover, a 3.46 Å distance (dashed line in Fig. 2) connects the Sn_4Se_{14} fragments to an infinite chain running along [001]. Hence we postulate that the steric effect of the larger cation in Ba_2SnSe_5 causes the more isolated Sn–Se fragments, and thereby different Sn–Se polyhedra.

The trimeric Sn_3Se_{10} unit of Ba_2SnSe_5 is composed of an irregular $SnSe_6$ octahedron in its center, with its Sn1–Se bonds ranging from 2.56 to 2.99 Å (Table 3). The various bond angles are close to the expected values, e.g., varying from 87.1° to 94.5° instead of the ideal 90° (Table 4). This octahedron is connected via two of its opposing basal edges to two Se_4 tetrahedra centered by the Sn2 and Sn3 atoms, which lines up the three Sn atoms of the Sn_3Se_{10} unit in an approximately linear arrangement (Fig. 2). These two tetrahedra are quite comparable to the third one, which is centered by Sn4. The $Sn4Se_4$ tetrahedron, the most regular one in this structure with Se–Sn–Se bond angles between 100.2° and 127.3°, does not share any Se atoms with the Sn_3Se_{10} unit. All Sn2–Se, Sn3–Se, and Sn4–Se bonds are in the range of 2.51–2.58 Å. These are expected lengths for Sn^{IV}–Se bonds; e.g., the isolated $Sn^{IV}Se_4$ tetrahedra of K_4SnSe_4 exhibit bonds between 2.49 and 2.53 Å [22]. An example for the uncommon octahedral Sn^{IV} coordination is found in the binary selenide $SnSe_2$ with six Sn–Se bonds of 2.68 Å per Sn atom [23], while the Sn1–Se bonds in Ba_2SnSe_5 average to 2.75 Å, with two

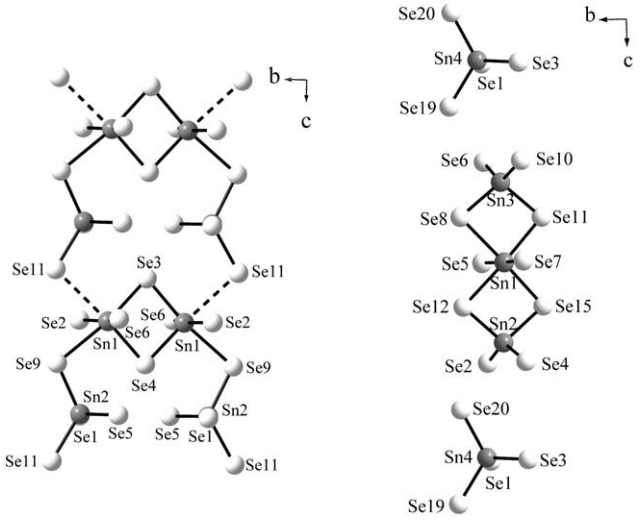

Fig. 2. Sn–Se polyhedra in Sr_2SnSe_5 (left) and Ba_2SnSe_5 (right).

Table 3
Selected Sn–Se and Se–Se distances (Å) of Ba_2SnSe_5

Sn1–Se7	2.5642(14)	Sn2–Se4	2.5097(15)
Sn1–Se5	2.5715(14)	Sn2–Se2	2.5196(15)
Sn1–Se15	2.7386(16)	Sn2–Se12	2.5721(15)
Sn1–Se11	2.7544(16)	Sn2–Se15	2.5778(16)
Sn1–Se12	2.8719(15)		
Sn1–Se8	2.9852(16)		
Sn3–Se10	2.5045(15)	Sn4–Se3	2.5279(13)
Sn3–Se6	2.5085(15)	Sn4–Se19	2.5311(15)
Sn3–Se8	2.5425(15)	Sn4–Se20	2.5327(15)
Sn3–Se11	2.5644(16)	Sn4–Se1	2.5548(14)
Se9–Se17	2.3828(17)	Se13–Se18	2.4372(17)
Se16–Se17	2.3794(17)	Se14–Se18	2.3780(17)

Table 4
Selected Se–Sn–Se and Se–Se bond angles [deg] of Ba_2SnSe_5

Se7–Sn1–Se5	176.67(5)	Se4–Sn2–Se2	137.85(6)
Se7–Sn1–Se15	91.74(5)	Se4–Sn2–Se12	105.09(5)
Se5–Sn1–Se15	91.23(5)	Se2–Sn2–Se12	106.47(5)
Se7–Sn1–Se11	89.43(5)	Se4–Sn2–Se15	100.14(5)
Se5–Sn1–Se11	91.83(5)	Se2–Sn2–Se15	101.26(5)
Se15–Sn1–Se11	94.51(4)	Se12–Sn2–Se15	99.78(5)
Se7–Sn1–Se12	88.96(5)		
Se5–Sn1–Se12	89.59(5)	Se10–Sn3–Se6	134.84(6)
Se15–Sn1–Se12	89.14(5)	Se10–Sn3–Se8	106.21(5)
Se11–Sn1–Se12	176.05(5)	Se6–Sn3–Se8	104.81(5)
Se7–Sn1–Se8	87.06(5)	Se10–Sn3–Se11	103.13(5)
Se5–Sn1–Se8	89.90(5)	Se6–Sn3–Se11	101.07(5)
Se15–Sn1–Se8	177.23(5)	Se8–Sn3–Se11	102.75(5)
Se11–Sn1–Se8	87.98(4)		
Se12–Sn1–Se8	88.34(4)	Se3–Sn4–Se19	102.85(5)
		Se3–Sn4–Se20	104.33(5)
Se9–Se17–Se16	110.64(7)	Se19–Sn4–Se20	116.80(5)
		Se3–Sn4–Se1	127.25(5)
Se13–Se18–Se14	108.27(6)	Se19–Sn4–Se1	100.21(5)
		Se20–Sn4–Se1	106.29(5)

shorter ones to the apices (2.56 Å, 2.57 Å), and the longer ones in the basal plane (2.74–2.99 Å).

The nominally six-coordinated Sn1 atom of Sr_2SnSe_5 exhibits a much more distorted coordination than the Sn1 of Ba_2SnSe_5, with two apical Sn–Se bonds of 2.52 and 2.54 Å, and four basal contacts of 2.64, 2.68, 3.11, and 3.46 Å. However, the latter may be neglected, leading to a five-fold (or 4 + 1) coordination of Sn1 in Sr_2SnSe_5. Noting that all Sn1–Se contacts of Ba_2SnSe_5 are shorter than 3 Å, we expect all of them to be bonding, and hence regard Sn1 as six-coordinated.

We calculated the bond valences (s) of these Sn–Se interactions via the Brown-Altermatt approach [24]:

$$s = \exp[(r_0 - r)/B],$$

with $r_0 = 2.527$ Å for Sn–Se bonds, and r being the actual bond distance. B was empirically determined to be 0.37 Å. These parameters worked rather well for the four-coordinated tetravalent Sn atoms, with summed bond valences of 3.82–3.98 per Sn atom (Sn2, Sn3, Sn4) in Ba_2SnSe_5. The four-coordinated Sn atom of Sr_2SnSe_5 has a valence of 3.91. As well, the six-coordinated Sn atom of $Sn^{IV}Se_2$ exhibits a valence (3.97) very close to the expected value of 4.0. On the other hand, the Sn1 atoms of both Sr_2SnSe_5 and Ba_2SnSe_5 have significantly smaller values, namely 3.68 and 3.58, respectively. Despite this, their calculated valences are clearly more indicative of Sn^{IV} than of Sn^{II}, as expected based on electron counting. (The trend observed indicates that a higher B value might be more appropriate.)

A different deviation from the common four-fold coordination of the Sn atoms was detected in monoclinic Ba_2SnTe_5 [10], while orthorhombic (kinetically stabilized) Ba_2SnTe_5 comprises exclusively four-coordinated Sn atoms [25]. The five-coordinated Sn3 atom of monoclinic Ba_2SnTe_5 exhibits three short Sn–Te bonds between 2.75 and 2.83 Å, and two longer ones of 3.00 and 3.39 Å. Its coordination sphere is best described as a trigonal bipyramid, with the two longer Sn–Te distances forming the apical bonds, and the three shorter ones the basal bonds. Again, we observe the same trend, i.e., that the higher coordinated Sn atom (here: Sn3) has a smaller totaled bond valence (using $r_0 = 2.735$ Å, $B = 0.37$ Å), namely 3.31 vs. 3.62 (Sn1) and 3.80 (Sn2).

In addition to these four isovalent tin polychalcogenides (Sr_2SnSe_5, Ba_2SnSe_5, and the two modifications of Ba_2SnTe_5) exhibiting four different Sn–Q coordination polyhedra, there are three different polychalcogenide groups, namely nonlinear Q_3^{2-} groups (Sr_2SnSe_5, Ba_2SnSe_5), Q_2^{2-} dumbbells (orthorhombic Ba_2SnTe_5), and nonclassical Q_5^{4-} groups in monoclinic Ba_2SnTe_5 (Fig. 3). The two symmetry-independent Se_3^{2-} groups of Ba_2SnSe_5 are almost identical, and compare well with the one of Sr_2SnSe_5. All these Se–Se bonds in both compounds are in the rather small range of 2.38–2.44 Å, and the bond angles are all typical, with 106–111°. These nonlinear groups, and the Te_2^{2-} group, are classical Zintl anions of the expected geometry with regular single bonds, allowing for a straightforward assignment of formal charges. The 34 valence-electrons of the Te_5^{4-} group with two central 'half bonds' (3.0 Å) and two terminal single bonds (2.8 Å) were assigned based on its structural analogy to the supposedly isoelectronic I_5^+ group of I_5AsF_6 [26] and the Te_5^{4-} group of NaTe [27]. The fact that Ba_2SnTe_5 exhibits a different polyanionic unit confirms the tendency of tellurides to show nonclassical hypervalent bonding, e.g., compounds like Cs_3Te_{22} [28] have no counterparts among the selenides.

3.2. Electronic structure

The densities of states (DOS curves) of Ba_2SnSe_5 and Sr_2SnSe_5 are being compared in Fig. 4. The energy windows start below the Se–p dominated domains, with the Fermi level separating the filled from the unfilled Se–p states. The latter stem from the antibonding Se–Se interactions. It is evident that the bandwidth of the filled states is smaller in case of Ba_2SnSe_5 (about 4.5 eV, compared to 5.5 eV in Sr_2SnSe_5). The larger band gap of Ba_2SnSe_5 (1.2 eV, compared to 0.9 eV) is a direct consequence of this difference, and it becomes visible by the dark-brownish color of Ba_2SnSe_5, vs. the black appearance of Sr_2SnSe_5. This trend can be qualitatively understood on the basis of the enlarged lattice parameters of Ba_2SnSe_5, compared to Sr_2SnSe_5, caused by the larger cation. Hence the secondary Se–Se interactions are generally longer in Ba_2SnSe_5, leading to smaller dispersions. For example, the Se_3^{2-} groups are

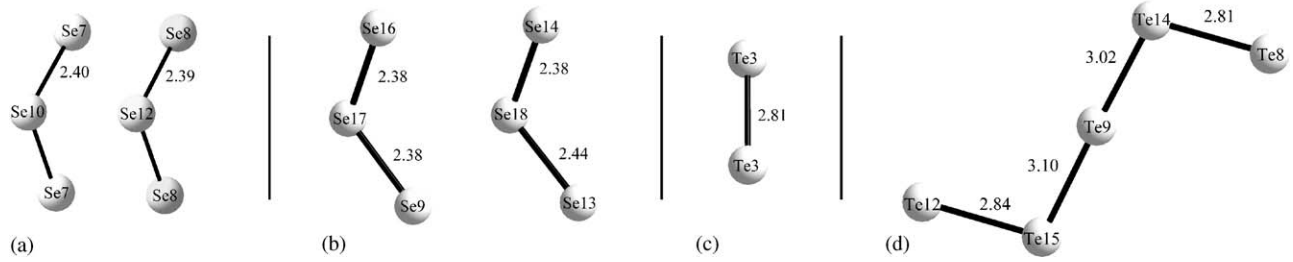

Fig. 3. Polychalcogenide units, from left to right: (a) the two Se_3^{2-} units of Sr_2SnSe_5; (b) the two Se_3^{2-} units of Ba_2SnSe_5; (c) the Te_2^{2-} unit of orthorhombic Ba_2SnTe_5; and (d) the Te_5^{4-} unit of monoclinic Ba_2SnTe_5.

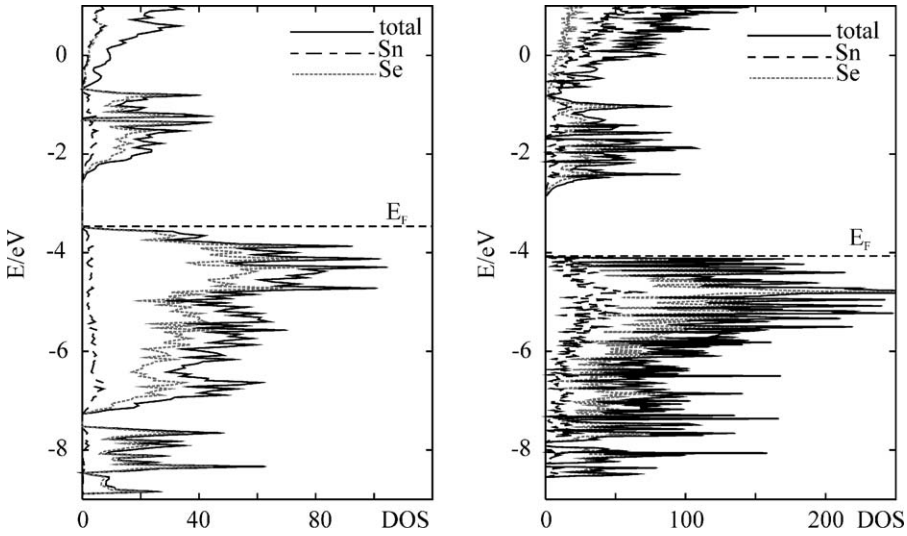

Fig. 4. Densities of States of Sr_2SnSe_5 (left) and Ba_2SnSe_5 (right). Dashed horizontal line: Fermi level (E_F).

stacked along the *c*-axis, in both structures, with intermolecular Se–Se distances of 3.58–3.76 Å in Ba_2SnSe_5, and 3.45–3.49 Å in Sr_2SnSe_5. The shortest Se–Se distances, aside from those of 2.4 Å in the Se_3^{2-} groups, are 3.41 Å in Ba_2SnSe_5 and 3.20 Å in Sr_2SnSe_5. Moreover, the band gap of monoclinic Ba_2SnTe_5 is significantly smaller, experimentally determined to be 0.18 eV, and computed to be 0.25 eV, because of the higher lying Te states, compared to the Se states.

We calculated the ICOHP [29] values of the different Sn–Se interactions of both Sr_2SnSe_5 and Ba_2SnSe_5 and the same for the Sn–Te interactions of the two Ba_2SnTe_5 modifications, to investigate whether the lengthier distances correspond to bonding interactions or not. The same was done for the *Q*–*Q* interactions within the polychalcogenides. For comparison, we plotted the relative ICOHP values in Fig. 5, i.e., the values divided by the one of the strongest interaction of that kind in that structure. In all cases, a strong bond strength—bond length correlation is apparent. All Se–Se and Sn–Se bonds <2.7 Å and Sn–Te bonds <2.9 Å are quite strong, being above 50% of the respective maximum. The Te–Te bonds may be divided into two kinds, the first being shorter than 2.9 Å, all (three) being above 88% of the strongest Te–Te bond, and the second one being between 3.0 and 3.1 Å, with relative strengths of 52% and 41%—supporting the classification into full and half bonds. The Sn–*Q* bonds become progressively weaker with increasing distance, with the Sn–Se curves running approximately parallel to the Sn–Te curves.

Where is the cut-off for the Sn–*Q* bonds? All bonds within the $SnSe_4$ tetrahedra of both polyselenides are shorter than 2.6 Å, and have relative ICOHPs of at least 81%. The two longest of the $Sn1Se_6$ octahedron of Ba_2SnSe_5 (2.87 and 2.99 Å) still exhibit 34% and 20%, respectively, of the strongest Sn–Se bond of Ba_2SnSe_5

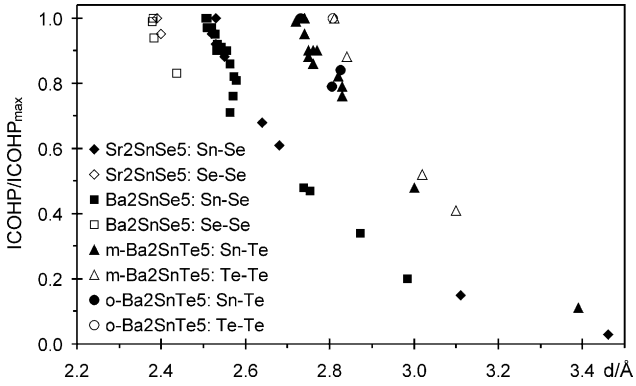

Fig. 5. Relative ICOHP values vs. interatomic distances of A_2SnQ_5 (A = Sr, Ba; Q = Se, Te).

(Sn3–Se10, 2.51 Å: ICOHP = −3.08 eV). This compares well to the 3.11 Å interaction of Sr_2SnSe_5 with 15%—numbers that most researchers will consider to be relevant. On the other hand, the 3.46 Å interaction of Sr_2SnSe_5 stands out with only 3%, as well as with a large length difference to the next shorter Sn–Se distance (0.35 Å). We therefore suggest to consider all Sn–Se interactions up to 3.11 Å as bonds (solid lines in Fig. 2), which leads to coordination numbers for the Sn atoms of 4 and 5 in Sr_2SnSe_5, and of 4 and 6 in Ba_2SnSe_5. In analogy, we propose to include all Sn–Te distances up to 3.4 Å, resulting in Sn coordination numbers of 4 and 5 in Ba_2SnTe_5.

3.3. Physical properties

Our electronic structure calculation of Ba_2SnSe_5 yielded a band gap of 1.2 eV, while the dark brown appearance is indicative of a gap at the edge of the visible range, 1.7 eV. This difference of 30% is not

atypical for LMTO calculations [30,31], as we found a 25% deviation in another barium selenide, $Ba_4La Ge_3SbSe_{13}$ [32].

Based on the band gap size >1 eV, one expects the resistivity for the undoped material to be large. Correspondingly, the resistance went out of scale in our measurement attempts, indicating a resistivity above 100 kΩ cm at room temperature.

4. Conclusion

The new polyselenide Ba_2SnSe_5 crystallizes in a new type that consists of nonlinear Se_3^{2-} units, distorted $Sn^{IV}Se_4$ tetrahedra and $Sn^{IV}Se_6$ octahedra. This differs from both modifications of Ba_2SnTe_5, where Te_2^{2-}, Te_5^{4-}, $Sn^{IV}Te_4$ tetrahedra and $Sn^{IV}Te_5$ trigonal bipyramids were found. Moreover, only four- and five-fold coordinated Sn^{IV} atoms occur in the recently published Sr_2SnSe_5. Our calculations show that all these Sn–Q interactions have bonding character.

The formation of different Sn–Se polyhedra in Ba_2SnSe_5, compared to Sr_2SnSe_5, appears to be a matrix effect, caused by the larger surrounding Ba^{2+} channels. On the other hand, the electronic differences between Se and Te atoms may be responsible for the different polyanionic units, which in turn lead to variations in the Sn–Q units.

Within this A_2SnQ_5 series, Ba_2SnSe_5 exhibits the largest band gap, computed to be 1.2 eV, and is the only material that is not black but dark brown. The band gaps are smaller in Sr_2SnSe_5 because of the shorter intermolecular Se–Se contacts leading to a higher band dispersion, and in Ba_2SnTe_5 because of the lower ionization potential of Te, compared to Se, leading to higher lying Te states.

Acknowledgments

Financial support from NSERC, CFI, OIT (Ontario Distinguished Researcher Award for H.K.), the Province of Ontario (Premier's Research Excellence Award for H.K.) and the Canada Research Chair program (CRC for H.K.) is appreciated.

References

[1] B.C. Sales, D. Mandrus, R.K. Williams, Science 272 (1996) 1325–1328.
[2] D.-Y. Chung, T. Hogan, P. Brazis, M. Rocci-Lane, C. Kannewurf, M. Bastea, C. Uher, M.G. Kanatzidis, Science 287 (2000) 1024–1027.
[3] R. Venkatasubramanian, E. Slivola, T. Colpitts, B. O'Quinn, Nature 413 (2001) 597–602.
[4] K.F. Hsu, S. Loo, F. Guo, W. Chen, J.S. Dyck, C. Uher, T. Hogan, E.K. Polychroniadis, M.G. Kanatzidis, Science 303 (2004) 818–821.
[5] D.-Y. Chung, T.P. Hogan, M. Rocci-Lane, P. Brazis, J.R. Ireland, C.R. Kannewurf, M. Bastea, C. Uher, M.G. Kanatzidis, J. Am. Chem. Soc. 126 (2004) 6414–6428.
[6] D.M. Rowe, CRC Handbook of Thermoelectrics, CRC Press, Boca Raton, FL, 1995.
[7] F.J. DiSalvo, Science 285 (1999) 703–706.
[8] J.O. Sofo, G.D. Mahan, Phys. Rev. B 49 (1994) 4565–4570.
[9] A. Assoud, N. Soheilnia, H. Kleinke, Chem. Mater. 16 (2004) 2215–2221.
[10] A. Assoud, S. Derakhshan, N. Soheilnia, H. Kleinke, Chem. Mater. 16 (2004) 4193–4198.
[11] P. Gutta, R. Hoffmann, Inorg. Chem. 42 (2003) 8161–8170.
[12] R. Pocha, D. Johrendt, Inorg. Chem. 43 (2004) 6830–6837.
[13] SAINT. Version 4 ed. Siemens Analytical X-ray Instruments Inc., Madison, WI, 1995.
[14] G.M. Sheldrick, SHELXTL. Version 5.12 ed, Siemens Analytical X-Ray Systems, Madison, WI, 1995.
[15] O.K. Andersen, Phys. Rev. B 12 (1975) 3060–3083.
[16] H.L. Skriver, The LMTO Method, Springer, Berlin, Germany, 1984.
[17] L. Hedin, B.I. Lundqvist, J. Phys. C 4 (1971) 2064–2083.
[18] P.E. Blöchl, O. Jepsen, O.K. Andersen, Phys. Rev. B 49 (1994) 16223–16233.
[19] R. Dronskowski, P.E. Blöchl, J. Phys. Chem. 97 (1993) 8617–8624.
[20] R.S. Mulliken, J. Chem. Phys. 23 (1955) 2343–2346.
[21] T. Hughbanks, R. Hoffmann, J. Am. Chem. Soc. 105 (1983) 3528–3537.
[22] K.O. Klepp, Z. Naturforsch. b47 (1992) 411–417.
[23] B. Palosz, E. Salje, J. Appl. Crystallogr. 22 (1989) 622–623.
[24] I.D. Brown, D. Altermatt, Acta Crystallogr. B 41 (1985) 244–247.
[25] J. Li, Y.Y. Liszewski, L.A. MacAdams, Chem. Mater. 8 (1996) 598–600.
[26] A. Apblett, F. Grein, J.P. Johnson, J. Passmore, P.S. White, Inorg. Chem. 25 (1986) 422–426.
[27] P.K. Böttcher, R., J. Less Comm. Met. 109 (1985) 311–321.
[28] W.S. Sheldrick, M. Wachhold, Angew. Chem. Int. Ed. Engl. 34 (1995) 450–451.
[29] G.A. Landrum, R. Dronskowski, Angew. Chem. Int. Ed. 39 (2000) 1560–1585.
[30] H. Yanagi, S.-I. Inoue, K. Ueda, H. Kawazoe, J. Appl. Phys. 88 (2000) 4159–4163.
[31] M. Tampier, D. Johrendt, Z. Anorg. Allg. Chem. 627 (2001) 312–320.
[32] A. Assoud, N. Soheilnia, H. Kleinke, J. Solid State Chem. 177 (2004) 2249–2254.